magnetochemistry

MDPI

Article

Multifunctional Synergistic Response Induced by Phase Transition in Molecular Compounds

Xiao-Feng Chen [1], Tao Wang [1], Dan Liao [1], Nan Wu [1], Yan Peng [1,*], Shi-Yong Zhang [2,*] and Zhao-Bo Hu [1,*]

[1] Jiangxi Provincial Key Laboratory of Functional Crystalline Materials Chemistry, Jiangxi University of Science and Technology, Ganzhou 341000, China; 6120220189@mail.jxust.edu.cn (X.-F.C.); 15779035038@163.com (T.W.); dan_liao1030@163.com (D.L.); 19972579477@163.com (N.W.)
[2] School of Chemistry and Chemical Engineering, Gannan Normal University, Ganzhou 341000, China
* Correspondence: yan.peng@jxust.edu.cn (Y.P.); zhsy1207@126.com (S.-Y.Z.); huzhaobo@smail.nju.edu.cn (Z.-B.H.)

Abstract: Two organic–inorganic materials $(TMAA)_2[CoCl_4]$ (**1**) and $(TMAA)_2[MnCl_4]$ (**2**) (TMAA = N,N,N-trimethyl-1-adamantylammonium hydroxide) were synthesized and characterized. It was found that both compounds exhibit first-order structural phase transition at high-temperature regions. As the temperature approaches the phase transition point, significant abnormal changes were observed in the dielectric properties and $\chi_M T$ values of compounds **1** and **2**. This phenomenon strongly highlights the dielectric bistable and spin bistable properties of compounds **1** and **2**. Further research shows that the dielectric constants of the compounds undergo significant changes upon the application of an external magnetic field, providing strong evidence for the existence of magnetic–dielectric coupling effects within compounds **1** and **2**.

Keywords: multifunctional synergistic response; spin bistability; dielectric; phase transitions

check for updates

Academic Editor: Carlos J. Gómez García

Received: 31 March 2025
Revised: 4 May 2025
Accepted: 6 May 2025
Published: 9 May 2025

Citation: Chen, X.-F.; Wang, T.; Liao, D.; Wu, N.; Peng, Y.; Zhang, S.-Y.; Hu, Z.-B. Multifunctional Synergistic Response Induced by Phase Transition in Molecular Compounds. *Magnetochemistry* **2025**, *11*, 41. https://doi.org/10.3390/magnetochemistry11050041

Copyright: © 2025 by the authors. Licensee MDPI, Basel, Switzerland. This article is an open access article distributed under the terms and conditions of the Creative Commons Attribution (CC BY) license (https://creativecommons.org/licenses/by/4.0/).

1. Introduction

Bistable materials are special materials whose physical properties can undergo reversible switching between different states when stimulated by external factors [1]. In traditional inorganic bistable materials, inorganic ferromagnets and ceramic ferroelectrics are the most widely studied [2–4]. The direction of magnetization in inorganic ferromagnets can be reversed by an external magnetic field, while the spontaneous polarization direction in ceramic ferroelectrics can be altered by an applied electric field. These bistable characteristics found broad applications in information processing and data storage. Over the past few decades, molecular bistable materials have attracted significant attention and been extensively studied within the scientific community [5–10]. Compared to traditional inorganic materials, molecular materials offer several advantages. First, their process is simpler, their structures are easier to control, and they are more environmentally friendly [11–17]. Second, the diversity of molecular structures and functions greatly expands the scope of bistability [18]. In molecular materials, bistable phenomena are not limited to ferromagnetic and ferroelectric properties, but also switchable magnetism [19,20]. In related studies, molecular bistable materials have gained significant interest from researchers, driven not only by a strong desire to understand the correlation between material properties and structures but also by the high expectation for developing next-generation high-performance functional materials [21], which are promising for applications in sensors [22,23], data storage [24,25], spintronics [26,27], displays [28,29], actuator devices [30,31], and so forth [32–37].

It is well known that the structure determines the physical properties of a material [38,39]. Therefore, changes in magnetic, electrical, optical, and other physical properties of a material are closely related to structural changes [40–44]. External stimuli such as temperature and light can trigger alterations in the spatial or electronic structure of the material, thereby modulating its physical properties [45–49]. Organic–inorganic hybrid materials consist of organic cationic guests and inorganic hosts, which can exhibit characteristics of both organic and inorganic materials [50]. For example, perovskites with the general formulae A_2BX_4 and ABX_3 (where A is an organic ammonium cation, B is a metal ion, and X is a halide ion) [51,52] can display varying magnetic, luminescent, ferroelectric, and dielectric properties depending on the compositions, and may even exhibit multiple physical properties simultaneously. For instance, the compound $(C_6H_5C_2H_3FNH_3)_2[MnCl_4]$ reported by us is capable of controlling fluorescence under a strong magnetic field, demonstrating a magneto-optical effect [52]. Therefore, it is anticipated that the structural phase transitions of organic–inorganic hybrid materials driven by temperature changes could enable the realization of multifunctional bistable effects.

Herein, two examples of inorganic–inorganic hybrid materials $(TMAA)_2[MCl_4]$ (M = Co (**1**) and Mn (**2**)) (TMAA = N,N,N-trimethyl-1-adamantylammonium hydroxide) were synthesized. Both compounds **1** and **2** exhibit a first-order structural phase transition at high temperatures. At the phase transition temperature, both the magnetic and dielectric properties of compounds **1** and **2** show bistable behavior. Moreover, when an in situ magnetic field is applied to compounds **1** and **2**, their dielectric constants undergo significant changes, which strongly suggests the presence of magneto-electric coupling effect in these compounds.

2. Materials and Methods

2.1. Materials

All chemicals and medications were acquired from reagent suppliers of Sigma Aldrich (Sigma Aldrich, St. Louis, MO, USA) and Innochem (Innochem, Beijing, China) without further purification. Powder X-ray diffraction (PXRD) was measured using Rigaku Miniflex 600 equipment (Rigaku Corporation, Tokyo, Japan) at a test angle of 5–50°. The phase purities of the samples employed in subsequent analyses were confirmed through powder X-ray diffraction (PXRD) characterization, which demonstrated excellent consistency with the simulated patterns derived from single-crystal X-ray diffraction data. The Elemental Vario EL analyzer (Elementar Analysensysteme GmbH, Langenselbold, Germany) was used to perform elemental analysis of compounds comprising C, H, and N. The complex dielectric constant ($\varepsilon = \varepsilon' - i\varepsilon''$) was measured using a TH2828A precision LCR meter (Tonghui Electronics Co., Ltd., Changzhou, China) equipped with temperature-controlled capabilities. The DC susceptibilities of compounds **1** and **2** were measured using a Quantum Design SQUID-based MPMS-3-type magnetometer (Quantum Design, Inc., San Diego, CA, USA). Magnetic data of compounds **1** and **2** were recorded in the temperature range of 2.0–430 K with a magnetic field of 1000 Oe. At the same time, in order to study the effect of phase transition on magnetism, the magnetic data changes during cooling and heating were recorded. The magnetization of compound **1** and **2** was recorded in field range of 0–7 T and at corresponding temperatures.

*2.2. Synthesis of $(TMAA)_2[CoCl_4]$ (**1**)*

$CoCl_2{\cdot}6H_2O$ (0.2379 g, 1 mmol) and TMAA (0.2113 g, 1 mmol) were dissolved in 10 mL of hydrochloric acid and stirred for 10 min. Then, the mixture was added into deionized water (10 mL). Solvent stirring for 10 min followed by filtration volatilization on a heating table at 40 °C gave blue-violet crystals after a few weeks. The yield of

$(TMAA)_2[CoCl_4]$ was 54% based on TMAA. FT-IR (KBr, cm^{-1}): 3852 (s), 3756 (s), 3649 (s), 2915 (s), 2858 (w), 1637 (w), 1555 (w), 1484 (m), 1374 (w), 1300 (w), 1231 (w), 1106 (w), 1036 (m), 948 (m), 838 (m), 568 (w), 456 (w). Calcd (%) for $C_{26}H_{48}Cl_4CoN_2 \cdot 2H_2O$: C, 49.93; H, 8.38; N, 4.48. wt% found: C, 50.06; H, 8.11; N, 4.39.

*2.3. Synthesis of $(TMAA)_2[MnCl_4]$ (**2**)*

Green crystals of complex **2** were synthesized in the same way as compound **1**, except that an equivalent amount of $MnCl_2$ was used in place of $CoCl_2 \cdot 6H_2O$. The yield of $(TMAA)_2[MnCl_4]$ was 63% based on TMAA. FT-IR (KBr, cm^{-1}): 3835 (w), 3738 (s), 3617 (s), 2917 (s), 2360 (w), 1920 (w), 1830 (w), 1701 (m), 1483 (s), 1360 (s), 1232 (m), 950 (s), 838 (s), 763 (w), 619 (s), 476 (m). Calcd (%) for $C_{26}H_{48}Cl_4MnN_2 \cdot H_2O$: C, 51.75; H, 8.36; N, 4.64. wt% found: C, 51.78; H, 8.18; N, 4.57.

2.4. X-Ray Single-Crystal Structure Determination

Single-crystal X-ray diffraction data were collected at different temperature using a Bruker D8 QUEST (Bruker Corporation, Billerica, MA, USA) diffractometer with Mo Kα radiation (λ = 0.71073 Å). Initial unit cell parameters were determined and data integration was performed using the APEX II software package. Structural solutions were obtained through intrinsic phasing methods implemented in SHELXT 2019, followed by full-matrix least-squares refinement against F^2 using SHELXL within the Olex2 interface. All non-hydrogen atoms were refined with anisotropic displacement parameters to achieve optimal structural models.

3. Results and Discussion

3.1. Structural Description

The structures of compounds **1** and **2** have been reported [52], and they are very similar to each other (Figure 1). The IR spectra and TG analyses were measured as shown in Figures S3 and S4. Therefore, in our detailed discussion of their structures, we will focus solely on compound **1** as a representative example. At a low temperature of 150 K, the crystal structure of compound **1** belongs to the monoclinic system, with the space group $P2_1/n$. The unit cell parameters are as follows: a = 8.9214(3) Å, b = 21.7558(8) Å, c = 14.7144(5) Å, β = 92.685(3)°, and Z = 4, with a unit cell volume V = 2852.81 (18) $Å^3$. At this temperature, the Co–Cl bond lengths fluctuate between 2.2742 Å and 2.2839 Å, while the Cl–Co–Cl bond angle ranges from 105.06° to 116.16° (Figure 1 and Table S2). At 340 K, some atoms are disordered, with the Co–Cl bond length ranging from 2.2661 Å to 2.2830 and the Cl–Co–Cl bond angle ranging from 104.87° to 116.26° (Table S2). Additionally, temperature-dependent powder X-ray diffraction (PXRD) patterns of compound **1** confirm the occurrence of a phase transition (Figure 2). Although the comparison between the high-temperature and low-temperature phases of compounds **1** and **2** shows no significant changes in the unit cell parameters, the $TMAA^+$ cation exhibits noticeable disorder as the temperature increases. Since the space group remains unchanged during the temperature variation, the phase transition is classified as an isostructural transition, with the intermediate phase assumed to be partially disorder. It is found that the rigid cyclic structure of $TMAA^+$ occupies a relatively large volume, with the terminal carbon atoms positioned at low-energy sites. This restricts atomic movement, allowing only small vibrations within a limited range [52].

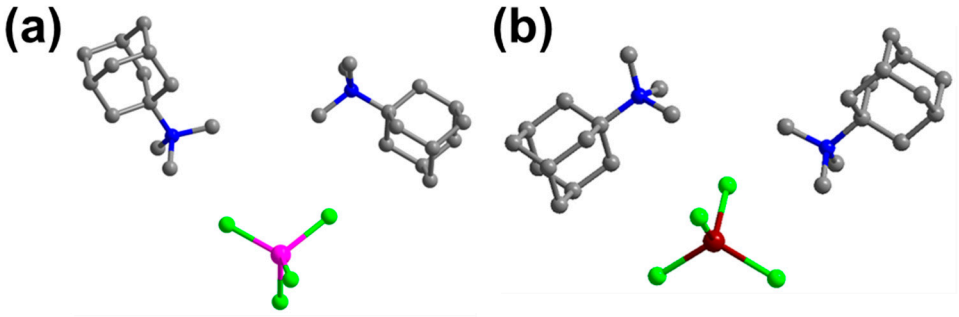

Figure 1. The molecular structures of **1** (**a**) and **2** (**b**). The pink, dark red, bright green blue, and gray spheres represent Co, Mn, Cl, N, and C atoms, respectively.

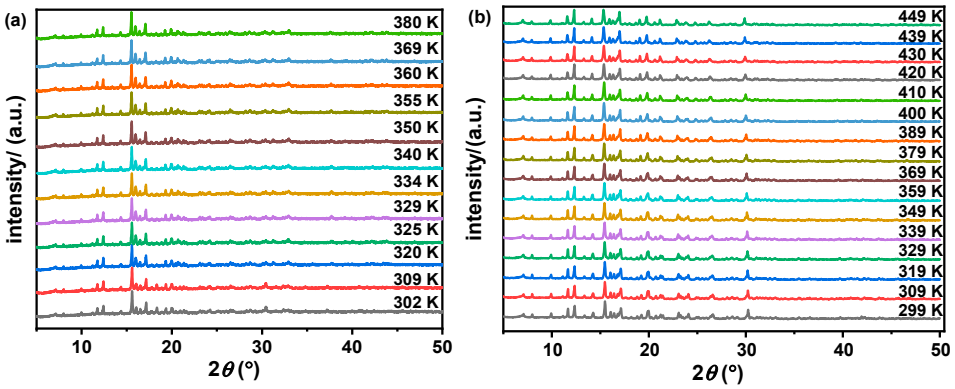

Figure 2. PXRD patterns of compounds **1** (**a**) and **2** (**b**) at variable temperatures.

3.2. Magnetic Properties

Variable-temperature dc magnetic susceptibility measurements were performed on polycrystalline samples of **1** and **2**. We conducted measurements of the molar magnetic susceptibility ($\chi_M T$) for compounds **1** and **2** over a temperature range of 2 to 300 K, under an external DC magnetic field of 1 kOe. As shown in Figure 3a, at room temperature, compound **1** exhibits a $\chi_M T$ value of 3.06 cm^3 K mol^{-1}, which is significantly higher than the theoretical value of 1.875 cm^3 K mol^{-1} for a single Co(II) ion (S = 3/2, g = 2.0). This discrepancy is attributed to the strong orbital contribution of the Co(II) ion [53,54]. Between 300 and 75 K, the $\chi_M T$ value for compound **1** remains nearly constant as the temperature decreases. Below 75 K, $\chi_M T$ drops sharply, reaching a minimum of 1.7 cm^3 K mol^{-1} at 2 K, which is attributed to the anisotropy of the Co(II) ion. We also measured the magnetic moment (M) as a function of magnetic field strength (H) for compound **1** over the full magnetic field range (0–7 T) at various temperatures (1.8, 2.5, 5.0, and 10 K). At 1.8 K and a magnetic field strength of 7 T, the magnetization of compound **1** reaches a maximum value of 2.35 μ_B, which is considerably lower than the theoretical saturation value of 3.0 μ_B for Co(II) ion (Figure 3a inset), further confirming the strong magnetic anisotropy present in compound **1**. For compound **2**, the $\chi_M T$ curve shows similar behavior to that of compound **1**, but with the key difference that Mn ions do not exhibit magnetic anisotropy. The $\chi_M T$ value for compound **2** at room temperature is 4.375 cm^3 K mol^{-1}, which is close to the theoretical value for Mn(II) ion (Figure 3b). As the temperature decreases, the $\chi_M T$ value for compound **2** remains constant until about 15 K. Below this temperature, $\chi_M T$ decreases rapidly, reaching a minimum value of 4.0 cm^3 K mol^{-1} at 2 K, due to zero-field splitting. At 1.8 K and a magnetic field of 7 T, the magnetization of compound **2** reaches its maximum value of 5.0 μ_B, approaching the saturation value for Mn(II) (Figure 3b inset). The DC magnetic susceptibility data for compounds **1** and **2** were fitted using the Hamiltonian operator in Formula 1 by PHI v3.1.6 software (Figure 3a,b) [55]. The

optimal fitting parameters obtained were g = 2.51, D = 14.48 cm^{-1}, E = 3.00 cm^{-1} and TIP = 4.9 × 10^{-4} cm^3 mol^{-1} for compound **1**; g = 1.99, D = 0.23 cm^{-1}, and TIP = 6.59 × 10^{-5} cm^3 mol^{-1} for compound **2**.

$$\hat{H} = D\left[\hat{S}_z^2 - \frac{S(S+1)}{3}\right] + g\mu_B SH \quad (1)$$

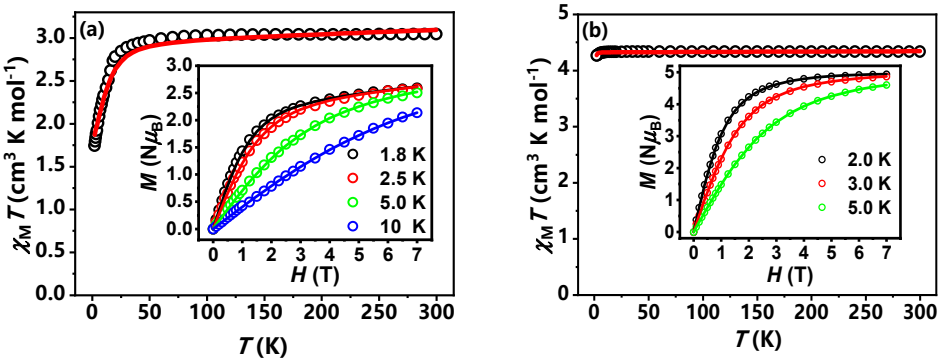

Figure 3. Variable-temperature dc susceptibility data of **1** (**a**) and **2** (**b**). Inset: Variable-temperature, variable-field dc magnetization data collected at different temperatures from 1 to 7 T. Solid lines indicate the best fits with the *PHI* program [55].

In order to investigate the magnetic bistability of compounds **1** and **2**, we measured the $\chi_M T$ vs. T curves of compounds **1** and **2** during the heating and cooling processes. As shown in Figure 4, two pairs of reversible heat anomalies were observed at 329 K/297 K and 359/343 K (heating/cooling, separately) for compound **1**, indicating two phase transitions at 329 K and 359 K for compound **1**. For compound **2**, the $\chi_M T$ remains almost unchanged before the phase transition temperature. When the temperature approaches the phase transition point, there is an abnormal change in the $\chi_M T$ value, which reaches their maximum value at 408 K. As heating continues, the $\chi_M T$ value remains almost unchanged at higher temperatures. Subsequently, as the temperature decreases, there is almost no change in the χ_MT value. During cooling, at 399 K, the minimum values of $\chi_M T$ reach 4.29 cm^3 K mol^{-1}. Then, as the temperature further decreases, the $\chi_M T$ value begins to stabilize, indicating only one phase transitions at 408 K for compound **2**.

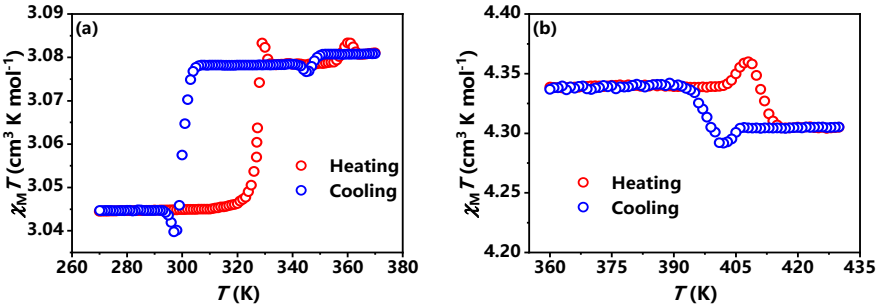

Figure 4. Temperature dependence of $\chi_M T$ vs. T during heating/cooling of **1** (**a**) and **2** (**b**) at high temperatures.

3.3. Dielectric Properties

The thermogravimetric analysis (TGA) curves of compounds **1** and **2** are shown in Figure S4. It can be seen from the figures that both compounds are decomposed at about 525 K, showing excellent thermal stability. The dielectric measurements of compounds **1** and **2** were obtained in the temperature range 300 to 430 K at 100 kHz (Figure S5). The value of ε' for compound **1** remains at 17.52 at LTP. When the temperature increases to 345 K, the

value of ε′ suddenly shows a step increase and reaches 45.91, which indicates an obvious dielectric abnormality. During the cooling process, the change in ε′ value is similar to that for heating process, indicating that compound **1** undergoes a reversible phase transition. For compound **2**, the value of ε′ is 3.19 at LTP, while it is 14.14 at 413.5 K. The abnormal change in ε′ value is attributed to the order–disorder transition of the $[TMAA]^+$ cations. Under an applied magnetic field, the peak of the curves does not change. However, the dielectric constant values decrease. The dielectric constant values decrease with a stronger magnetic field (Figure 5). This kind of physical phenomenon has been reported, but it is still a challenge to give a precise reason. However, it is clear that the magnetic field leads to such behavior probably through Lorentzian force, a slight change in the structure of paramagnetic compounds and/or the Hall effect.

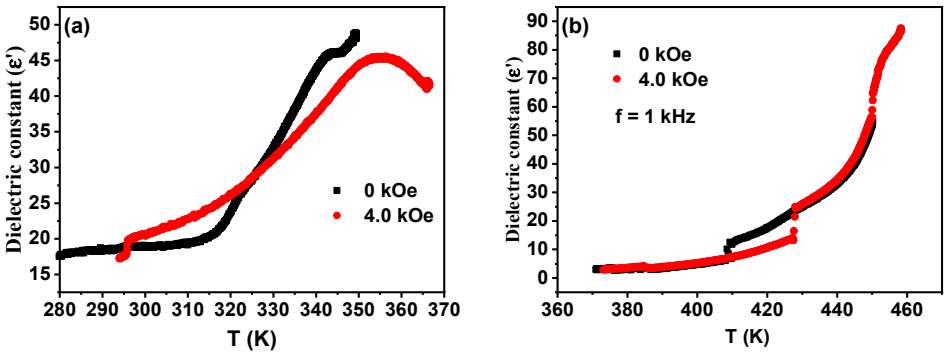

Figure 5. Dielectric curves of compounds **1** (**a**) and **2** (**b**) at different magnetic fields.

4. Conclusions

Two organic–inorganic hybrid materials $(TMAA)_2[CoCl_4]$ (**1**) and $(TMAA)_2[MnCl_4]$ (**2**) were synthesized through the reaction between N,N,N-Trimethyladamantan-1-aminium hydroxide and cobaltous chloride/manganese chloride. Both compounds show a first structure transition at high temperature, owing to the order–disorder character of the phase transition. Both compounds show a magnetic and dielectric response. Compound **1** has two-step spin bistability, while **2** only displayed one-step spin bistability. Both compounds demonstrated magnetoelectric coupling at high temperature. This study demonstrates that organic–inorganic hybrids are multifunctional synergistically responsive materials with the induction of phase transitions in molecular compounds.

Supplementary Materials: The following supporting information can be downloaded at https://www.mdpi.com/article/10.3390/magnetochemistry11050041/s1: Figure S1: Packing picture of compounds **1** (a) and **2** (b); Figure S2: (a) The molecular structures of **1@340** at 340 K. The pink, bright green blue and gray spheres represent Co, Cl, N and C atoms, respectively. (b) Packing picture of compounds **1@340** at 340 K. Red lines indicate hydrogen bonds; Figure S3: The IR spectra of compounds **1** and **2**; Figure S4: TG analysis diagram of compounds **1** (a) and **2** (b). Figure S5. Dielectric curves of compounds **1** (a) and **2** (b) at 100 kHz. Table S1: Crystallographic data and structural refinement parameters for compounds **1**, **1@340** and **2**; Table S2: Bond lengths [Å] and angles [°] for compounds **1**, **1@340** and **2**.

Author Contributions: The manuscript was prepared with the contributions of all authors. X.-F.C.: Synthesis, IR, TG and single-crystal X-ray diffraction studies; T.W.: Dielectric property characterization and synthesis; D.L.: PXRD; N.W.: Magnetic property characterization and writing—original draft; S.-Y.Z.: Magnetic and dielectric property characterization; Y.P. and Z.-B.H.: Careful follow-up and improvement of the manuscript, general idea and plan for the publication. All authors have read and agreed to the published version of the manuscript.

Funding: National Natural Science Foundation of China (22261022, 22161002 and 22105089), Natural Science Foundation of Jiangxi Province (20224BAB214005 and 20242BAB23018), Jiangxi Provincial Key Laboratory of Functional Crystalline Materials Chemistry (2024SSY05161) and Double Thousand Talents Program in Jiangxi Province (jxsq2020101087).

Institutional Review Board Statement: Not applicable.

Informed Consent Statement: Not applicable.

Data Availability Statement: CCDC 2115536–2115539 contain the supplementary crystallographic data for complexes **1** and **2**, respectively. These data can be obtained free of charge via http://www.ccdc.cam.ac.uk/conts/retrieving.html (accessed on 4 May 2025) or from Cambridge Crystallographic Data Centre (12 Union Road, Cambridge CB2 1EZ, UK; fax: (+44) 1223-336-033; or e-mail: deposit@ccdc.cam.ac.uk). The original contributions presented in the study are included in the article and Supplementary Materials; further inquiries can be directed to the corresponding authors.

Acknowledgments: We would like to acknowledge the Nantong University Analytical Testing Center for its support for testing.

Conflicts of Interest: The authors declare no conflicts of interest.

References

1. Sato, O. Dynamic molecular crystals with switchable physical properties. *Nat. Chem.* **2016**, *8*, 644–656. [CrossRef] [PubMed]
2. Wang, J.; Neaton, J.B.; Zheng, H.; Nagarajan, V.; Ogale, S.B.; Liu, B.; Vihland, D.; Vaithyanathan, V.; Schlom, D.G.; Waghmare, U.V.; et al. Epitaxial $BiFeO_3$ Multiferroic Thin Film. *Heterostruct. Sci.* **2003**, *299*, 1719–1722.
3. Fiebig, M.; Lottermoser, T.; Meier, D.; Trassin, M. The evolution of multiferroics. *Nat. Rev. Mater.* **2016**, *1*, 16046. [CrossRef]
4. Feng, Z.W.; Shi, T.; Geng, G.Z.; Li, J.J.; Deng, Z.L.; Kivshar, Y.; Li, X.P. Dual-band polarized upconversion photoluminescence enhanced by resonant dielectric metasurfaces. *eLight* **2023**, *3*, 21. [CrossRef]
5. Sun, B.; Liu, X.F.; Li, X.Y.; Cao, Y.; Yan, Z.; Fu, L.; Tang, N.J.; Wang, Q.; Shao, X.F.; Yang, D.Z.; et al. Reversible Thermochromism and Strong Ferromagnetism in Two-Dimensional Hybrid Perovskites. *Angew. Chem. Int. Ed.* **2020**, *59*, 203–208. [CrossRef]
6. Liu, J.Y.; Zhang, S.Y.; Zeng, Y.; Shu, X.; Du, Z.Y.; He, C.T.; Zhang, W.X.; Chen, X.M. Molecular Dynamics, Phase Transition and Frequency-Tuned Dielectric Switch of an Ionic Co-Crystal. *Angew. Chem. Int. Ed.* **2018**, *130*, 8164–8168. [CrossRef]
7. Jia, Z.H.; Liu, J.Y.; Liu, D.X.; Zhang, S.Y.; Du, Z.Y.; He, C.T.; Zhang, W.X.; Chen, X.M. Four-step thermosensitive dielectric response arising from motionable low-symmetry ammonium confined in deformable supramolecular cages. *J. Mater. Chem. C* **2021**, *9*, 8076–8082. [CrossRef]
8. Wang, C.F.; Wang, N.; Shi, C.; Ye, H.Y.; Zhang, Y.; Miao, L.P. NH_4^+/K^+-substitution-induced C–F–K coordination bonds for designing the highest-temperature hybrid halide double perovskite ferroelastic. *Chin. Chem. Lett.* **2023**, *34*, 107774. [CrossRef]
9. Wang, C.F.; Wang, N.; Liu, L.; Miao, L.P.; Ye, H.Y.; Zhang, Y.; Shi, C. Enantiomeric hybrid high-temperature multiaxial ferroelectrics with a narrow bandgap and high piezoelectricity. *Chin. Chem. Lett.* **2023**, *34*, 108051. [CrossRef]
10. Liu, S.M.; He, L.; Wang, Y.Z.; Shi, P.P.; Ye, Q. Tunable phase transition, band gap and SHG properties by halogen replacement of hybrid perovskites [(thiomorpholinium)PbX_3, X = Cl, Br, I]. *Chin. Chem. Lett.* **2022**, *33*, 1032–1036. [CrossRef]
11. Garcia, V.; Bibes, M. Inside story of ferroelectric memories. *Nature* **2012**, *483*, 279–280. [CrossRef] [PubMed]
12. Harada, J.; Kawamura, Y.; Takahashi, Y.; Uemura, Y.; Hasegawa, T.; Taniguchi, H.; Maruyama, K. Plastic/Ferroelectric Crystals with Easily Switchable Polarization: Low-Voltage Operation, Unprecedentedly High Pyroelectric Performance, and Large Piezoelectric Effect in Polycrystalline Forms. *J. Am. Chem. Soc.* **2019**, *141*, 9349–9357. [CrossRef] [PubMed]
13. Liao, W.Q.; Zeng, Y.L.; Tang, Y.Y.; Peng, H.; Liu, J.C.; Xiong, R.G. Multichannel Control of Multiferroicity in Single Component Homochiral Organic Crystals. *J. Am. Chem. Soc.* **2021**, *143*, 21685–21693. [CrossRef] [PubMed]
14. Liu, K.; Ouyang, B.; Guo, X.J.; Liu, Y. Advances in flexible organic field-effect transistors and their applications for flexible electronics. *Npj Flex. Electron.* **2022**, *6*, 1. [CrossRef]
15. Liu, Y.; Wang, S.; Chen, Z.J.; Xiao, L.X. Applications of ferroelectrics in photovoltaic devices. *Sci. China Mater.* **2016**, *59*, 851. [CrossRef]
16. Tang, Y.Y.; Li, P.F.; Liao, W.Q.; Shi, P.P.; You, Y.M.; Xiong, R.G. Multiaxial Molecular Ferroelectric Thin Films Bring Light to Practical Applications. *J. Am. Chem. Soc.* **2018**, *140*, 8051–8059. [CrossRef]
17. Wei, X.K.; Domingo, N.; Sun, Y.; Balke, N.; Dunin-Borkowski, R.E.; Mayer, J. Progress on Emerging Ferroelectric Materials for Energy Harvesting, Storage and Conversion. *Adv. Energy Mater.* **2022**, *12*, 2201199. [CrossRef]
18. Zhang, W.; Xiong, R.G. Ferroelectric Metal–Organic Frameworks. *Chem. Rev.* **2012**, *112*, 1163–1195. [CrossRef]
19. Horiuchi, S.; Tokura, Y. Organic ferroelectrics. *Nat. Mater.* **2008**, *7*, 357–366. [CrossRef]

20. Gui, L.A.; Chen, J.W.; Zhang, Y.F.; Li, L.H.; Li, J.R.; Hu, Z.B.; Zhang, S.Y.; Zhang, J.L.; Zhang, Z.Y.; Ye, H.Y.; et al. Room-temperature Magnetocapacitance Spanning 97 K Hysteresis in Molecular Material. *Angew. Chem. Int. Ed.* **2025**, *64*, e202416380. [CrossRef]
21. Gui, L.A.; Zhang, Y.F.; Peng, Y.; Hu, Z.B.; Song, Y. Synergetic Responses of Multiple Functions Induced by Phase Transition in Molecular Materials. *ChemPhysChem* **2024**, *25*, e202400297. [CrossRef] [PubMed]
22. Zhang, Z.X.; Zhang, T.; Shi, P.P.; Zhang, W.Y.; Ye, Q.; Fu, D.W. Exploring high-performance integration in a plastic crystal/film with switching and semiconducting behavior. *Inorg. Chem. Front.* **2020**, *7*, 1239–1249. [CrossRef]
23. Gao, Y.F.; Zhang, Z.X.; Zhang, T.; Su, C.Y.; Zhang, W.Y.; Fu, D.W. Regulated molecular rotor in phase transition materials with switchable dielectric and SHG effect. *Mater. Chem. Front.* **2020**, *4*, 3003–3012. [CrossRef]
24. Li, X.Q.; Li, D.; Peng, Y.; Liu, Y.; Wang, J.Q.; Li, L.N.; Yao, Y.P.; Liu, X.T.; Luo, J.H. Exploring a layered iodide perovskite crystal with centimetered dimension for extended spectral polarization-sensitive photodetection. *J. Mater. Chem. C* **2021**, *9*, 9499–9504. [CrossRef]
25. Jia, J.H.; Li, Q.W.; Chen, Y.C.; Liu, J.L.; Tong, M.L. Luminescent single-molecule magnets based on lanthanides: Design strategies, recent advances and magneto-luminescent studies. *Coord. Chem. Rev.* **2019**, *378*, 365–381. [CrossRef]
26. Liu, K.; Zhang, X.J.; Meng, X.X.; Shi, W.; Cheng, P.; Powell, A.K. Constraining the coordination geometries of lanthanide centers and magnetic building blocks in frameworks: A new strategy for molecular nanomagnets. *Chem. Soc. Rev.* **2016**, *45*, 2423–2439. [CrossRef]
27. Zhang, Z.X.; Su, C.Y.; Li, J.; Song, X.J.; Fu, D.W.; Zhang, Y. Ferroelastic Hybrid Bismuth Bromides with Dual Dielectric Switches. *Chem. Mater.* **2021**, *33*, 5790–5799. [CrossRef]
28. Su, C.Y.; Lun, M.M.; Chen, Y.D.; Zhou, Y.C.; Zhang, Z.X.; Chen, M.; Huang, P.Z.; Fu, D.W.; Zhang, Y. Hybrid Optical-Electrical Perovskite Can Be a Ferroelastic Semiconductor. *CCS Chem.* **2022**, *4*, 2009–2019. [CrossRef]
29. Zhang, S.Y.; Shu, X.; Zeng, Y.; Liu, Q.Y.; Du, Z.Y.; He, C.T.; Zhang, W.X.; Chen, X.M. Molecule-based nonlinear optical switch with highly tunable on-off temperature using a dual solid solution approach. *Nat. Commun.* **2020**, *11*, 2752. [CrossRef]
30. Gao, F.F.; Li, X.; Qin, Y.; Li, Z.G.; Guo, T.M.; Zhang, Z.Z.; Su, G.D.; Jiang, C.Y.; Azeem, M.; Li, W.; et al. Dual-Stimuli-Responsive Photoluminescence of Enantiomeric Two-Dimensional Lead Halide Perovskites. *Adv. Opt. Mater.* **2021**, *9*, 2100003. [CrossRef]
31. Liu, X.L.; Li, D.; Zhao, H.X.; Dong, X.W.; Long, L.S.; Zheng, L.S. Inorganic–Organic Hybrid Molecular Materials: From Multiferroic to Magnetoelectric. *Adv. Mater.* **2021**, *33*, 2004542. [CrossRef] [PubMed]
32. Tang, Y.Y.; Wang, Z.X.; Li, P.F.; You, Y.M.; Stroppa, A.; Xiong, R.G. Brilliant triboluminescence in a potential organic–inorganic hybrid ferroelectric: $(Ph_3PO)_2MnBr_2$. *Inorg. Chem. Front.* **2017**, *4*, 154–159. [CrossRef]
33. Jin, W.H.; Lu, H.H.; Zhang, Q.; Qu, D.H. A dual-mode orthogonally tunable fluorescent system covering the whole white light region. *Mater. Chem. Front.* **2020**, *4*, 532–536. [CrossRef]
34. Wang, Z.P.; Zhang, Z.Z.; Tao, L.Q.; Shen, N.N.; Hu, B.; Gong, L.K.; Li, J.R.; Chen, X.P.; Huang, X.Y. Hybrid Chloroantimonates(III): Thermally Induced Triple-Mode Reversible Luminescent Switching and Laser-Printable Rewritable Luminescent Paper. *Angew. Chem. Int. Ed.* **2019**, *58*, 9974–9978. [CrossRef]
35. Li, J.; Xu, C.; Zhang, W.Y.; Shi, P.P.; Ye, Q.; Fu, D.W. Smart and efficient opto-electronic dual response material based on two-dimensional perovskite crystal/thin film. *J. Mater. Chem. C* **2020**, *8*, 1953–1961. [CrossRef]
36. Morita, H.; Tsunashima, R.; Nishihara, S.; Inoue, K.; Omura, Y.; Suzuki, Y.; Kawamata, J.; Hoshino, N.; Akutagawa, T. Ferroelectric Behavior of a Hexamethylenetetramine-Based Molecular Perovskite Structure. *Angew. Chem. Int. Ed.* **2019**, *58*, 9184–9187. [CrossRef]
37. Zhang, Y.F.; Gui, L.A.; Peng, Y.; Hu, Z.B.; Song, Y. Perspective on room temperature and low-field-induced magnetoelectric coupling in molecular complexes. *Dalton Trans.* **2025**, *54*, 881–888. [CrossRef]
38. Clark, J.B.; Hastie, J.W.; Kihlborg, L.H.E.; Metselaar, R.; Thackeray, M.M. Definitions of terms relating to phase transitions of the solid state. *Pure Appl. Chem.* **1994**, *66*, 577–594. [CrossRef]
39. Shi, C.; Han, X.B.; Zhang, W. Structural phase transition-associated dielectric transition and ferroelectricity in coordination compounds. *Coord. Chem. Rev.* **2019**, *378*, 561–576. [CrossRef]
40. Du, Z.Y.; Xu, T.T.; Huang, B.; Su, Y.J.; Xue, W.; He, C.T.; Zhang, W.X.; Chen, X.M. Switchable Guest Molecular Dynamics in a Perovskite-Like Coordination Polymer toward Sensitive Thermoresponsive Dielectric Materials. *Angew. Chem. Int. Ed.* **2015**, *12*, 928–932. [CrossRef]
41. Muhammad; Lim, C.W. From Photonic Crystals to Seismic Metamaterials: A Review via Phononic Crystals and Acoustic Metamaterials. *Arch. Comput. Method. E* **2022**, *29*, 1137–1198. [CrossRef]
42. Nishita, M.; Park, S.Y.; Nishio, T.; Kamizaki, K.; Wang, K.; Takumi, T.; Hashimoto, R.; Otani, H.; Pazour, G.J.; Hsu, V.W.; et al. Ror2 signaling regulates Golgi structure and transport through IFT20 for tumor invasiveness. *Sci. Rep.* **2017**, *7*, 1. [CrossRef] [PubMed]
43. Sen, A.; Swain, D.; Guru Row, T.N.; Sundaresan, A. Unprecedented 30 K hysteresis across switchable dielectric and magnetic properties in a bright luminescent organic-inorganic halide $(CH_6N_3)_2MnCl_4$. *J. Mater. Chem. C* **2019**, *7*, 4838–4845. [CrossRef]

44. Zhang, Y.; Ye, H.Y.; Cai, H.L.; Fu, D.W.; Ye, Q.; Zhang, W.; Zhou, Q.H.; Wang, J.L.; Yuan, G.L.; Xiong, R.G. Switchable Dielectric, Piezoelectric, and Second-Harmonic Generation Bistability in a New Improper Ferroelectric above Room Temperature. *Adv. Mater.* **2014**, *26*, 4515. [CrossRef]
45. Schmid, H. Some symmetry aspects of ferroics and single phase multiferroics. *J. Phys. Condens. Matter.* **2008**, *20*, 434201. [CrossRef]
46. Spaldin, N.A.; Fiebig, M.; Mostovoy, M. The toroidal moment in condensed-matter physics and its relation to the magnetoelectric effect. *J. Phys. Condens. Matter.* **2008**, *20*, 434203. [CrossRef]
47. Yao, H.Q.; Ding, Z.J.; Zhang, S.Y.; Wu, Y.F.; Qiu, X.; Peng, Y.; Ye, H.Y.; Hu, Z.B. High temperature synergistic response of magnetism, dielectricity, and luminescence in a Mn(II)-based molecular organic–inorganic hybrid. *CrystEngComm* **2024**, *26*, 1767–1772. [CrossRef]
48. Yao, H.Q.; Li, L.H.; Zhang, S.Y.; Peng, Y.; Liu, S.J.; Wen, H.R.; Zhang, J.L.; Ye, H.Y.; Song, Y.; Hu, Z.B. Near-Room-Temperature Synergetic Response of Magnetism, Dielectricity and Luminescence Based on $(C_5NH_{13}Cl)_2MnBr_4$. *Chem. Eur. J.* **2023**, *29*, e202300598. [CrossRef]
49. Cheng, Y.; Ruan, H.P.; Peng, Y.; Li, L.H.; Xie, Z.Q.; Liu, L.; Zhang, S.Y.; Ye, H.Y.; Hu, Z.B. Magnetic, dielectric and luminescence synergetic switchable effects in molecular material $[Et_3NCH_2Cl]_2[MnBr_4]$. *Chin. Chem. Let.* **2024**, *35*, 108554. [CrossRef]
50. Zhao, X.H.; Huang, X.C.; Zhang, S.L.; Shao, D.; Wei, H.Y.; Wang, X.Y. Cation-Dependent Magnetic Ordering and Room-Temperature Bistability in Azido-Bridged Perovskite-Type Compounds. *J. Am. Chem. Soc.* **2013**, *135*, 16006–16009. [CrossRef]
51. Du, S.N.; Su, D.; Ruan, Z.Y.; Zhou, Y.Q.; Deng, W.; Zhang, W.X.; Sun, Y.; Liu, J.L.; Tong, M.L. Reversible Switchability of Magnetic Anisotropy and Magnetodielectric Effect Induced by Intermolecular Motion. *Angew. Chem. Int. Ed.* **2022**, *61*, e202204700. [CrossRef] [PubMed]
52. Shao, T.; Ren, R.Y.; Huang, P.Z.; Ni, H.F.; Su, C.Y.; Fu, D.W.; Xie, L.Y.; Lu, H.F. Metal ion modulation triggers dielectric double switching and green fluorescence in A_2MX_4-type compounds. *Dalton Trans.* **2022**, *51*, 2005–2011. [CrossRef] [PubMed]
53. Hu, Z.B.; Gui, L.A.; Li, L.H.; Xiao, T.T.; Hand, A.T.; Tin, P.; Ozerov, M.; Peng, Y.; Ouyang, Z.; Wang, Z.; et al. Co^{II} Single-ion Magnet and its Multi-dimensional Aggregations: Influence of the Structural Rigidity on Magnetic Relaxation Process. *Chin. Chem. Lett.* **2025**, *36*, 109600. [CrossRef]
54. Li, L.H.; Peng, Y.; Zhang, S.; Xiao, T.; Song, Y.; Ye, H.Y.; Zhang, J.; Zhang, Y.Q.; Wang, Z.; Hu, Z.B. Subtle changes Effect on Slow Relaxation Behaviour of Co(II) Ions Based Metal Organic Frameworks. *Cryst. Growth Des.* **2023**, *23*, 2099–2105. [CrossRef]
55. Chilton, N.F.; Anderson, R.P.; Turner, L.D.; Soncini, A.; Murray, K.S. PHI: A powerful new program for the analysis of anisotropic monomeric and exchange-coupled polynuclear d- and f-block complexes. *J. Comput. Chem.* **2013**, *34*, 1164–1175. [CrossRef]

Disclaimer/Publisher's Note: The statements, opinions and data contained in all publications are solely those of the individual author(s) and contributor(s) and not of MDPI and/or the editor(s). MDPI and/or the editor(s) disclaim responsibility for any injury to people or property resulting from any ideas, methods, instructions or products referred to in the content.